ACS OMEGA

http://pubs.acs.org/journal/acsodf

Article

α,ε-Hybrid Peptide-Stabilized Magnetic Nanoparticle-Coated Paper-Based Actuators

Ananda Shit, Surajit Singh, Olamilekan Joseph Ibukun, Milan Gumtya, and Debasish Haldar*

Cite This: *ACS Omega* 2023, 8, 8712−8721

Read Online

ACCESS | Metrics & More | Article Recommendations | Supporting Information

ABSTRACT: The development of α,ε-hybrid peptide-stabilized magnetic nanoparticles and their application to fabricate a paper-based actuator has been reported. From single-crystal diffraction analysis, the nitropeptide **2** has an extended structure with a *trans* geometry. The one-pot in situ multiple oxidation−reduction reaction of a synthetic nitropeptide solution in ammonium hydroxide and $FeCl_2$ leads to the formation of Fe_3O_4 nanoparticles. The reduction reaction replaces the nitro group with an amine group, which finally acts as capping agent for the stabilization of the Fe_3O_4 nanoparticles. Paper-based soft magneto machines with multivariant actuation modes such as contraction−expansion, bending, and uplifting locomotion have been studied. The device has potential as controllable paper-based soft robots.

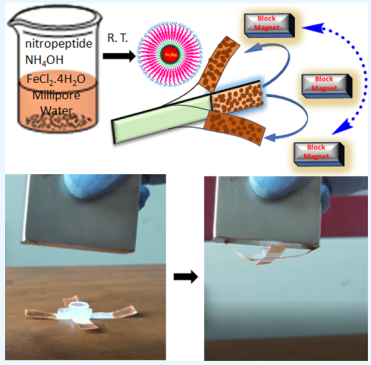

INTRODUCTION

Over the past decade, scientists have been fascinated by the development of stimulus-responsive soft materials and their potential applications as soft actuators.[1] The soft actuators can convert external stimuli into mechanical work.[2] The soft actuators have great potential in the fabrication of intelligent devices like smart switches, soft robots, artificial muscles, and various micro-electromechanical systems.[3] The most important feature of soft actuators is both programmable and controllable shape deformation.[4] From the literature, external stimuli, such as pH,[5] solvent vapors,[6] electricity,[7] light,[8] magnetic fields,[9] heat,[10] and humidity,[11] have been exploited to manipulate soft actuators.[12−14]

A wide range of stimulus-responsive soft materials, such as hydrogels,[15] organogels, electroactive polymers,[16] shape-memory polymers[17] plastic crystals, dielectric elastomers,[18] self-healing crystals,[19] etc., have been used for the design of soft actuators with reversible and fast deformation propensities.[20−22]

Synthetic foldamers containing designer building blocks are regularly used to mimic the structure and function of biopolymers.[23−25] The incorporation of noncoded β-, γ-, δ-, or ε-amino acids into folded structures with α-amino acid chains has been widely used in the design of foldamers having hybrid backbones.[26−29] For example, Gopi and co-workers have reported the unsaturated amino acid-triggered folding of polypeptides.[30] However, controlling the molecular orientation and diverse degrees of self-assembly of unsaturated peptides in comparison with their saturated analogues is still challenging.[30]

Herein we have synthesized two nitropeptides containing *trans*-α,β-unsaturated ε-amino acid and α-amino acids. The natural existence and very good bioactivities of unsaturated amino acids motivated us to examine the conformational preferences of these amino acids in hybrid peptides. Although 3-(3-aminophenyl)propionic acid has been extensively investigated in biology and materials science,[19,20] very little is known about the conformational properties of the unsaturated analogue 3-nitrocinnamic acid. 2-Aminoisobutyric acid (Aib) is helicogenic and conformationally rigid. 3-Nitrocinnamic acid is also geometrically constrained. L-Leu or L-Phe will adjust the hydrophobicity (Figure 1). Interestingly, the α,ε-hybrid

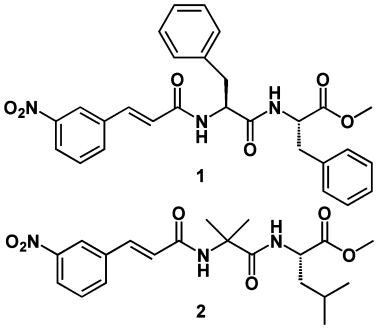

Figure 1. Chemical structures of α,ε-hybrid nitropeptides **1** and **2**.

Received: December 20, 2022
Accepted: February 14, 2023
Published: February 24, 2023

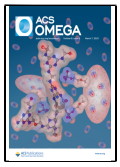

peptides **1** and **2** exhibit extended *trans* conformations in the solid state. The one-pot in situ multiple oxidation−reduction reaction of a synthetic nitropeptide solution in ammonium hydroxide and $FeCl_2$ leads to the formation of Fe_3O_4 nanoparticles. The reduction reaction replaces the nitro group with an amine group, which finally acts as capping agent for the stabilization of the Fe_3O_4 nanoparticles. Paper-based soft magneto machines with multivariant actuation modes such as contraction−expansion, bending, and uplifting locomotion has been studied.

EXPERIMENTAL SECTION

General. All L-amino acids (L-phenylalanine, 2-amino-isobutyric acid, L-leucine), *m*-nitro benzaldehyde, and malonic acid were purchased from Sigma chemicals. HOBt (1-hydroxybenzotriazole), DCC (dicyclohexylcarbodiimide), $FeCl_3{\cdot}6H_2O$ (ferric chloride hexahydrate), and $FeSO_4{\cdot}7H_2O$ (ferrous sulfate heptahydrate) were purchased from SRL.

Peptide Synthesis. Peptide **1** and peptide **2** were synthesized by the traditional solution-phase method.[31] The amino acid C-terminus was protected by methyl ester formation. Coupling was promoted by 1-ethyl-3-(3-(dimethylamino)propyl) carbodiimide (EDC). The purification of products was done using column chromatography on silica gel (mesh size 100−200) with an *n*-hexane−ethyl acetate solution as eluent. The reaction intermediates and final peptides were fully characterized by ^{1}H NMR (400 and 500 MHz) spectroscopy, ^{13}C NMR (125 MHz) spectroscopy, mass spectrometry, and FT-IR spectroscopy analyses. Further, X-ray crystallography was performed to characterize the peptide **2**.

Synthesis of NH_2-Phe-Phe-OMe. 0.852 g (2 mmol) of Boc-NH-Phe-Phe-OMe was taken in a 25 mL round-bottom (RB) flask and mixed with 2.5 mL of trifluoroacetic acid (TFA) to dissolve it completely, and the reaction mixture was stirred at room temperature for 8 h. TFA was evaporated from the solution by heating it at around 80 °C using a heating mantle. The semi-solid residue was treated with 20 mL of diethyl ether to remove the impurities (unreacted Boc-NH-Phe-Phe-OMe and 2-methylpropene) through the filtrate part by filtration using whatman-40 filter paper. The white residue powder was collected to yield NH_2-Phe-Phe-OMe, which was then directly used for the next step without any further purification and for spectroscopic characterization. The product was greyish white colored with yield of 0.610 g (1.43 mmol, 72%).

*Synthesis of Peptide **1**.* 3-(3-Nitrophenyl)-acrylic acid (0.84 g, 5 mmol) was dissolved in 25 mL of dichloromethane (DCM) in an ice−water bath. NH_2-Phe-Phe-OMe was isolated from 1.17 g (10 mmol) of the corresponding salt andtrifluoroacetate ester by neutralization and subsequent extraction with ethyl acetate. The ethyl acetate extract was removed in a vacuum and then added to the reaction mixture, immediately followed by 1.344 g (7 mmol) of 1-ethyl-3-(3-(dimethylamino)propyl) carbodiimide (EDC) and 0.95 g (7 mmol) of HOBt. The reaction mixture was allowed to come to room temperature and stirred for 48 h. DCM was evaporated, and the residue was dissolved in ethyl acetate (60 mL). The organic layer was washed with 2 M HCl (3 × 50 mL), brine (2 × 50 mL), 1 M sodium carbonate (3 × 50 mL), and brine (2 × 50 mL) and dried over anhydrous sodium sulfate. Purification was done by a silica gel column (100−120 mesh size) with an ethyl acetate and hexane mixture (1:5) as the eluent. The product was obtained as white flake solids with the yield of 1.3 g (3 mmol, 60%). ^{1}H NMR (400 MHz, DMSO-d_6, δ ppm): 8.62−8.60 (d, 1H, Phe-NH proton), 8.37 (m, 2H, Ar-H), 8.35−8.33 (d, 1H, Phe-NH proton), 7.99−7.97 (d, 1H, Ar-H), 7.72−7.68 (t, 1H, Ar-H), 7.49−7.45 (d, 1H, vinylic proton), 7.29−7.15 (m, 10H, Ar-H), 6.91−6.87 (d, 1H, vinylic Proton), 4.76−4.70 (m, 1H, Phe C_αH), 4.55−4.50 (m, 1H, PheC_αH), 3.60 (s, 3H, ester-CH_3 proton), 3.09−3.05 (m, 1H, Phe-C_βH), 3.05−2.99 (m, 1H, Phe-C_βH), 2.99−2.94 (m, 1H, Phe-C_βH), 2.80−2.74 (m, 1H, Phe-C_βH). ^{13}C NMR (125 MHz, DMSO-d_6, δ ppm): 172.22, 164.55, 148.79, 138.12, 137.55, 137.24, 132.02, 54.14, 52.42, 38.26, 37.13. ESI-MS (MeOH): $C_{28}H_{27}N_3O_6$ m/z = 501.29; $[M + Na]^+$ = (calculated) 524.19, (found) 524.78; $[2M + Na]^+$ = 1026.3087. FT-IR spectral data: 3286 cm^{-1} (N−H stretching), 3085 cm^{-1} (C−H stretching), 1731 cm^{-1} (C═O stretching), 1633 cm^{-1} (amide I stretching), 1540 cm^{-1} (amide II bending).

*Synthesis of Peptide **2**.* *m*-Nitrocinnamic acid (MNCA) containing peptide (MNCA-Aib−OH) (2.92 g, 10 mmol) was dissolved in 50 mL of DCM in an ice−water bath. NH_2-Leu-OMe was isolated from 1.72 g (12 mmol) of the corresponding salt and methyl ester by neutralization and subsequent extraction with ethyl acetate, and the ethyl acetate extract was removed in a vacuum and then added to the reaction mixture, followed immediately by 3.16 g (16.5 mmol) of 1-ethyl-3-(3-(dimethylamino)propyl) carbodiimide hydrochloride (EDC) and 2.3 g (16.5 mmol) of HOBt. The reaction mixture was allowed to come to room temperature and stirred for 48 h. DCM was evaporated, and the residue was dissolved in ethyl acetate (60 mL). The organic layer was washed with 2 M HCl (3 × 50 mL), brine (2 × 50 mL), 1 M sodium carbonate (3 × 50 mL), and brine (2 × 50 mL) and dried over anhydrous sodium sulfate. It was evaporated in a vacuum to yield MNCA-Aib-Leu-OMe. Purification was done by silica gel column (100−120 mesh size) with an ethyl acetate and hexane mixture (1:4) as the eluent. The product was obtained as white solid powder with the yield of 1.7 g (4.2 mmol, 46%). The product was characterized by NMR, mass spectrometry and IR spectroscopy. ^{1}H NMR (400 MHz, DMSO-d_6, δ ppm): 8.34 (t, 1H, Ar-H), 8.19−8.17 (m, 1H, Ar-H), 7.77−7.75 (m, 1H, Ar-H), 7.64−7.60 (d, 1H, J = 16 Hz, vinylic-H), 7.57−7.53 (t, 1H, Ar-H), 6.93−6.91 (d, 1H, J = 8 Hz, Leu-NH proton), 6.66 (s, 1H, Aib-NH proton), 6.60−6.56 (d, 1H, J = 16 Hz, vinylic-H), 4.63−4.58 (m, 1H, Leu-CαH), 3.73 (s, 3H, OMe proton), 1.69−1.61 (m, 9H, Leu-C_β, Leu-Cγ, Aib-C_β proton), 0.95−0.93 (d, 6H, J = 8 Hz, Leu-C_δ proton). ^{13}C NMR (125 MHz, DMSO-d_6, δ ppm): 174.28, 173.47, 164.74, 148.72, 143.86, 138.62, 136.59, 133.88, 129.98, 124.18, 121.98, 57.76, 52.41, 51.23, 41.45, 121.98, 57.76, 24.93, 22.89, 22.03. Mass spectral data TOF-MS m/z: Mol. Wt. = 405.45, $[M + Na]^+$ = 428.37; $[M + K]^+$ = 444.38, $[2M + Na]^+$ = 833.39. FT-IR spectral data: 3280 cm^{-1} (N−H stretching), 2955 cm^{-1} (C−H stretching), 1740 cm^{-1} (ester C═O stretching), 1663 cm^{-1} (amide I), 1526 cm^{-1} (amide II).

Synthesis of Magnetic Nanoparticles. The magnetic nanoparticles were synthesized by the one-pot oxidation−reduction reaction and centrifugation technique.[12] Under an inert atmosphere, an $FeCl_2{\cdot}4H_2O$ solution in degassed Milli-Q water (resistivity of 18.2 MΩ-cm) was added to the ammonium hydroxide solution of corresponding nitropeptide. In presence of ammonium hydroxide, $FeCl_2$ converted to $Fe(OH)_2$, which was further oxidized to $Fe(OH)_3$ by the nitropeptide. Finally, Fe_3O_4 nanoparticles were developed by the reaction between $Fe(OH)_2$ and $Fe(OH)_3$. The reduction reaction replaces the nitro group with an amine group, which

https://doi.org/10.1021/acsomega.2c08092
ACS Omega 2023, 8, 8712−8721

finally acts as a capping agent for the stabilization of the Fe_3O_4 nanoparticles (Figure 2). The black precipitate was washed

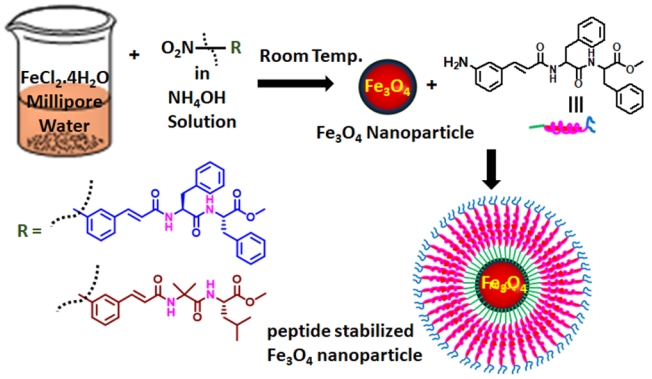

Figure 2. Schematic presentation of the synthesis of magnetic nanoparticles (peptide **1**−Fe_3O_4 and peptide **2**−Fe_3O_4).

with Millipore water several times, centrifuged, washed with ethanol to remove loosely assembled peptides, and dried under vacuum for 48 h. For our reference, we also synthesized pure Fe_3O_4 magnetic nanoparticles (without peptide capping) by following a traditional coprecipitation method (Figure S1).[36]

Coating of Nanoparticles on Paper. A α,ε-hybrid peptide-stabilized Fe_3O_4 nanoparticle suspended in methanol was dropcasted uniformly on one side of a paper strip using a microtip and a spatula. It was dried for 24 h at room temperature, followed by vacuuming. It was placed in a static position with help of a clam, and the whole system was kept in a nonmagnetic zone. Hence, when the solvent (methanol) was evaporated, the paper strip was coated by the peptide−nanoparticle conjugates. The same method was performed for pure Fe_3O_4 nanoparticles.

NMR Experiments. All NMR spectroscopy was done on a 400 MHz Jeol or 500 MHz Bruker spectrometer. Compound concentrations were in the 1−10 mM range in DMSO-d_6 and $CDCl_3$ solutions.[31]

FT-IR Experiments. FT-IR spectroscopy in the solid state was performed with a PerkinElmer Spectrum RX1 spectrophotometer using the KBr disk method.

Mass Spectrometry. Mass spectrometry was carried out on a Waters Corporation Q-Tof Micro YA263 high-resolution mass spectrometer by electrospray ionization (positive mode).

Field Emission Scanning Electron Microscopy. Field emission-scanning electron microscopy (FE-SEM) was performed to examine the morphologies of the peptide-stabilized nanoparticles. 2 mg of the corresponding compound was dispersed in 1 mL of methanol, and the solution was

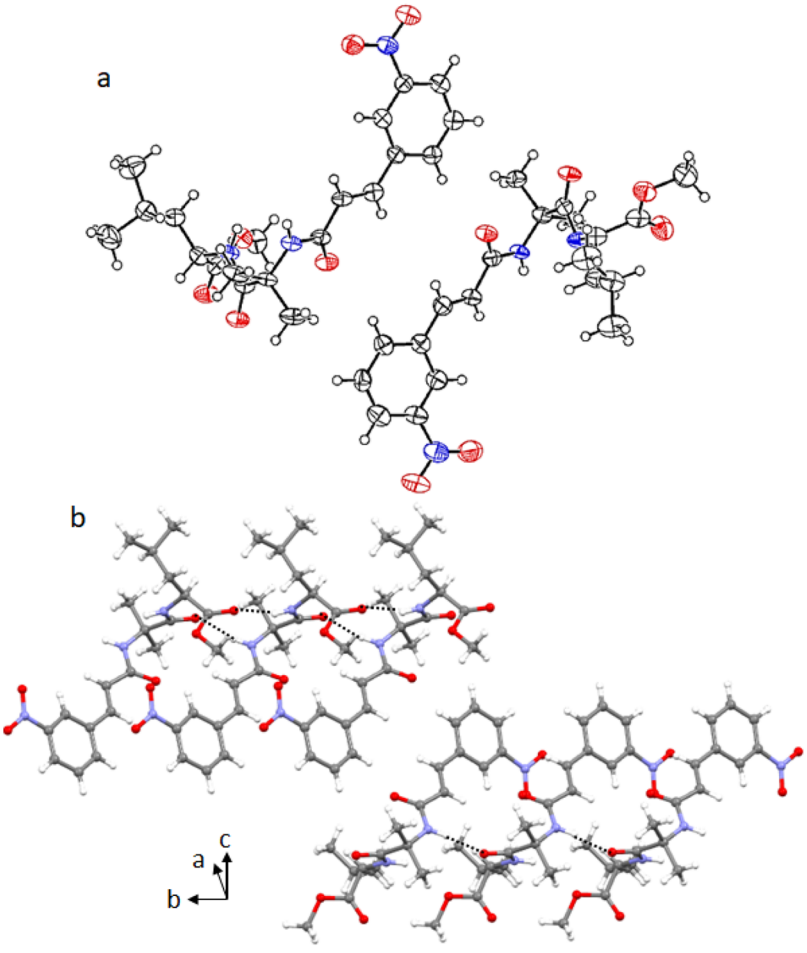

Figure 3. (a) Oak Ridge Thermal-Ellipsoid Plot Program (ORTEP) diagram of α,ε-hybrid peptide foldamer **2** showing the antiparallel arrangement of molecules (50% probability). (b) Higher-order assembly of α,ε-hybrid peptide foldamer **2** to form an antiparallel arrangement. Black dotted lines represent intermolecular hydrogen bonding.

https://doi.org/10.1021/acsomega.2c08092
ACS Omega 2023, 8, 8712−8721

dropcasted on microscopic glass coverslip and dried under vacuum for 48 h. The samples were gold-coated with a sputter, and the images were captured in an FE-SEM apparatus (JEOL Scanning Microscope-JSM-6700F).

DLS Study. Particle sizes were measured by dynamic light scattering (DLS) using a Malvern Zeta Sizer Nano ZS instrument (Malvern Instruments Ltd., UK) equipped with a He−Ne laser (wavelength of 633 nm). First, we made a 10^{-2} M stock-suspended solution in methanol. Then we made a 10^{-4} M solution in the respective solvent (methanol). For the DLS size measurement, we took 20 μL of the respective mixture in 1 mL of solvent with a respective solution ratio.

Powder X-ray Diffraction (PXRD) Study. The PXRD pattern was recorded in a Rigaku X-ray diffractometer (C 3000) with a parallel beam optics attachment. The instrument was operated at a 45 kV voltage and 200 mA current and was calibrated with a standard silicon sample. The wavelength of the X-ray source is 1.5418 Å (Kα value of Cu). The compound was ground for 1 min to obtain a fine powder sample with the help of a mortar and pastel. Then, the powder sample was subjected to place in a glass sample holder, and the holder was placed into the instrument horizontally to measure the PXRD data.

X-ray Crystallography. Diffraction-quality white-colored crystals of peptide **2** were obtained from mixture of solvent (methanol−water with 3:1 ratio) by slow evaporation. Intensity data were collected with Mo Kα radiation by a Bruker APEX-2 CCD diffractometer. Data were processed using the Bruker SAINT package. The structure solution and refinement were performed by SHELX97. Refinement of non-hydrogen atoms was performed using anisotropic thermal parameters.[31] Crystal data of peptide **2** are as follows: formula, $C_{20}H_{27}N_3O_6$; formula weight, 405.45; space group, *I*2; a = 20.2472(5) Å; b = 5.8735(1) Å; c = 36.0878(11) Å; α = 90°; β = 101.032(3)°; γ = 90°; V = 4212.32(18); Z = 8; D = 1.279 g·cm^{-3}; K = 100; R_1 = 0.0744; and wR_2 = 0.2178. The data were submitted at the Cambridge Crystallographic Data Centre with CCDC reference 2206018.

RESULTS AND DISCUSSION

The noncoded amino acid *trans*-3-nitrocinnamic acid was synthesized by the condensation reaction between 3-nitrobenzaldehyde and malonic acid in a DMF−water medium at 120 °C for 6 h. The α,ε-hybrid peptides **1** and **2** were synthesized using a traditional solution-phase peptide coupling reaction using EDC as a coupling reagent (Scheme S1 and Scheme S2). The synthesized peptides and intermediates were purified by column chromatography and analyzed by ^{1}H NMR, ^{13}C NMR, FT-IR, and mass spectrometry.

First, the structure and the assembly of unsaturated peptides were investigated by solid-state FT-IR spectroscopy. The unsaturated α,ε-hybrid peptide **1** exhibits N−H stretching vibrations at 3290 cm^{-1} for hydrogen-bonded NHs. There is also non-hydrogen bonded N−H at 3447 cm^{-1}. The ester peak appears at 1731 cm^{-1} ,and amide I and amide II peaks appear at 1636 and 1540 cm^{-1} (Figure S2a).[21] However, the α,ε-hybrid peptide **2** shows a N−H stretching vibration at 3280 cm^{-1} for hydrogen-bonded NHs and amide I and amide II peaks at 1663 and 1526 cm^{-1} (Figure S2b).[21] Hence the peptides adopt a hydrogen-bonded sheet-like structure.

To explore the molecular conformation and self-assembly pattern of the 3-nitroocinnamic acid-containing α,ε-hybrid peptides, single-crystal X-ray analysis was performed. White colored monoclinic crystals of peptide **2** were obtained from a methanol−water (3:1) solution by slow evaporation. There are two molecules of peptide **2** in the asymmetric unit (Figure 3a) in the antiparallel arrangement.[22] The two molecules are stabilized by four intermolecular N−H···O hydrogen bonds between Aib N−H and Aib C═O and Leu N−H and Leu C═O (Figure S3). The formation of self-assembled dimer of peptides **1** and **2** was also confirmed by ESI-MS spectrometry (Figure S4). In higher-order packing, the peptide **2** molecules self-assemble to form an antiparallel arrangement (Figure 3b) through intermolecular hydrogen bonding interactions. Table 1 shows the hydrogen bonding parameters of peptide **2**. Due to

Table 1. Hydrogen Bonding Parameters of Peptide 2[a]

D−H···A	D···H (Å)	H···A (Å)	D···A (Å)	D−H···A (Å)
N2−H2···O4[a]	0.8800	1.9500	2.818(8)	167
N5−H5···O10[b]	0.8800	2.0000	2.870(8)	168
N6−H6A···O11[b]	0.8800	2.2100	3.054(8)	162

[a]Symmetry equivalent: a = x, −1 + y, z; b = x, 1 + y, z.

the presence of multiple benzene rings and the strong hydrophobic properties of the phenylalanine moieties in peptide **1**, it probably could not form an ordered structure. We have tried to crystallize peptide **1** from different solutions but failed to obtain an X-ray-quality crystal.

The morphology of the peptides was investigated by POM and field emission scanning electron microscopy (FE-SEM) (Figure S5). The FE-SEM images show that the peptides **1** and **2** exhibit a polydisperse microsphere morphology (Figure S5). The average diameter of peptide **1** microspheres is about 1 μm, but the average diameter of peptide **2** microspheres is about 1.5 μm.

In general, Fe_3O_4 nanoparticles can be synthesized using different methods and can be modified or stabilized by different capping agents; in addition, to control high surface activity and high specific surface area, different surfactants can be used.[32] However, there are only a few examples showing one-pot, low-cost, and efficient in situ multiple oxidation−reduction reactions of synthetic nitropeptides to develop Fe_3O_4 nanoparticles.[33] Here we have used two unsaturated nitropeptides that can act as oxidizing agents for the synthesis and stabilization of magnetic nanoparticles. Hence, there is no need for any other external agent or surfactant to fabricate Fe_3O_4 nanoparticles. Moreover, the presence of L-Phe, Aib, and L-Leu moieties will help to enrich the hydrophobicity around the Fe_3O_4 nanoparticle as well as the attachment process on the paper surface by various noncovalent interactions such as hydrogen bonding, $\pi-\pi$ interaction, and hydrophobic interactions, which might be more effective in the diverse filed of actuation.[34] In this regard, we have synthesized peptide **1**−Fe_3O_4 nanoparticles, peptide **2**−Fe_3O_4 nanoparticles, and pure Fe_3O_4 nanoparticles.

All three types of Fe_3O_4 nanoparticles were analyzed and characterized by different spectroscopic studies. The morphology of α,ε-hybrid peptide-stabilized magnetic nanoparticles was further studied by field emission-scanning electron microscopy (FE-SEM) techniques. The FE-SEM images (Figure 4) depict the formation of peptide-stabilized Fe_3O_4 nanoparticles. From Figure 4a, the average diameter of peptide **1**−Fe_3O_4 nanoparticles is combined average (ca.) 95 nm. In the case of peptide **2**−Fe_3O_4 and pure Fe_3O_4 nanoparticles, the average diameters are 67 and 35 nm, respectively (Figure S6).

https://doi.org/10.1021/acsomega.2c08092
ACS Omega 2023, 8, 8712−8721

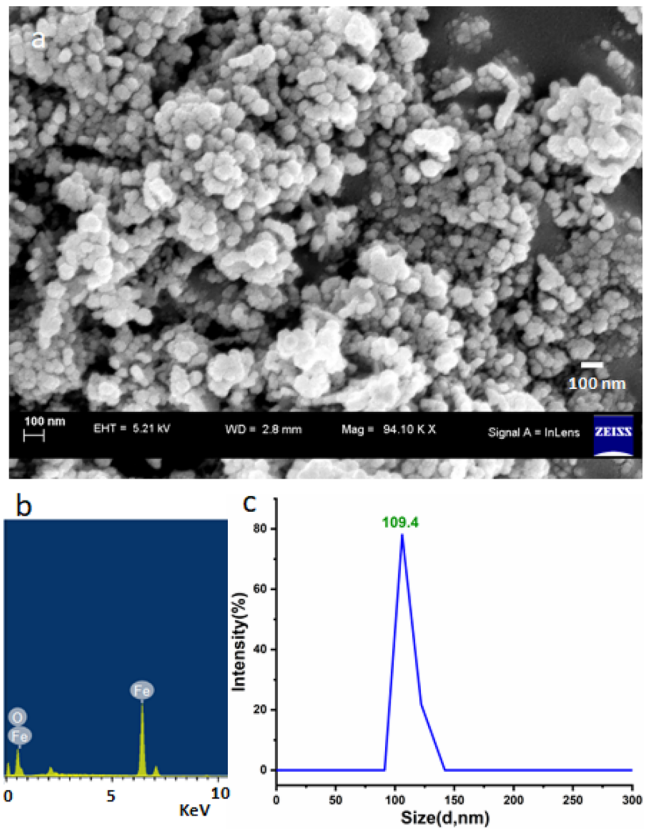

Figure 4. (a) FE-SEM image of α,ε-hybrid peptide **1**−Fe_3O_4 magnetic nanoparticles. (b) EDS spectrum of α,ε-hybrid peptide **1**−Fe_3O_4 nanoparticles. (c) DLS study of magnetic nanoparticles prepared and stabilized by peptide **1**.

Peptide **1** contains two phenylalanine (-Phe) residues, whereas peptide **2** contains one 2-aminoisobutyric acid (-Aib) residue and another Leucine (-Leu) residue in its peptide backbone. The hydrophobicity as well as the self-assembly of these two peptides around Fe_3O_4 nanoparticles are different, which indicates that grafted peptide **1** stabilized nanoparticles with a larger average diameter compared to peptide **2**, as seen from the average diameter of the pure Fe_3O_4. Peptide-stabilized Fe_3O_4 nanoparticles are of a larger average size than pure Fe_3O_4, which might be due to grafting of peptide residues on the surface of Fe_3O_4 magnetic nanoparticles.

Energy-dispersive X-ray spectroscopy (EDS) experiments were done for the metal content determination of the α,ε-hybrid peptide-stabilized magnetic nanoparticles. Figure 4b displays the elemental composition of α,ε-hybrid peptide **1**−Fe_3O_4 magnetic nanoparticles, verifying the presence of Fe and O. The quantitative determination of the metal content was found to be 78.13 weigh t% Fe and 21.87 weight % O.

Dynamic light scattering (DLS) experiments were performed to assess the size of the magnetic nanoparticles.[14] DLS is a rapid screening method used to define nanostructures by the presence of discrete peak intensity. From the DLS study in suspended methanol solution, it was found that peptide−Fe_3O_4 nanoparticles prepared and stabilized by α,ε-hybrid peptides have hydrodynamic sizes between 90 an 150 nm, with average sizes ca. 109 ± 6.91 nm for peptide **1**−Fe_3O_4 nanoparticles (Figure 4C) and 91.65 ± 5.81 nm for peptide **2**−Fe_3O_4 nanoparticles. (Figure S7). However, the particle sizes varied for different peptides due to the assembly of the peptides and aggregation. The peptide-stabilized magnetic nanoparticles are superparamagnetic in nature. Hence, the NMR experiments could not be carried out for further characterization.

However, FT-IR spectroscopy is an excellent technique for studying the α,ε-hybrid peptide-stabilized magnetic nanoparticles. The interactions between peptides and Fe_3O_4 can be analyzed by the change in the FT-IR spectra. Figure 5 shows

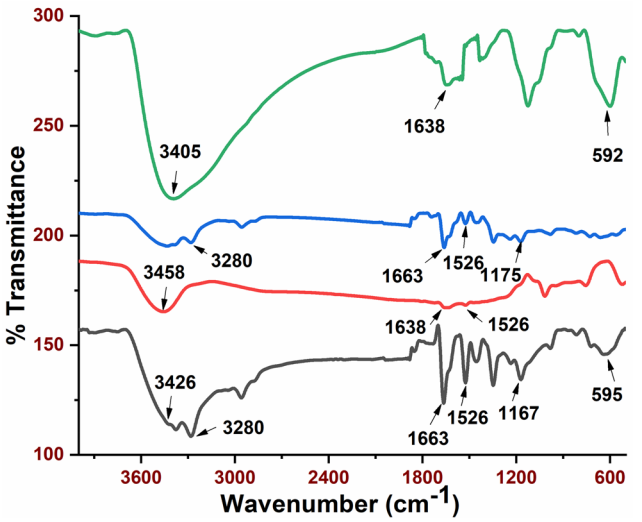

Figure 5. FT-IR absorption spectra. Black, pure peptide **2**−pure Fe_3O_4; red, peptide **2**−Fe_3O_4 nanoparticle; blue, pure peptide **2**; green, pure Fe_3O_4.

stacked FT-IR spectra of different Fe_3O_4 magnetic nanoparticles combined with peptide **2**. The spectrum exhibits an absorption peak above 3400 cm^{-1}, which represents the stretching vibration of O−H in H_2O, and peaks around 592 cm^{-1}, which denote the stretching vibration of the Fe−O bond in Fe_3O_4. The peak at 1638 cm^{-1} represents the bending vibration of H_2O. As a control, pure peptide **2** and pure Fe_3O_4 nanoparticles were mixed physically (pure peptide **2**−pure Fe_3O_4), and the spectrum was measured. The characteristic bands of peptide at 1526 cm^{-1} (amide II) are present in all the spectrum except pure Fe_3O_4. The stretching vibration of the C═O bond at 1663 cm^{-1} (amide I), which is present in pure peptide **2** and pure peptide **2**−pure Fe_3O_4, is absent in case of peptide **2**−Fe_3O_4 NPs (nanoparticles). The NH stretching frequency at 3280 cm^{-1} for peptide **2** and the stretching vibration of the C−O bond at 1175 cm (pure peptide **2**) and 1167 cm^{-1} (pure peptide **2** - pure Fe_3O_4) are also absent in peptide **2**−Fe_3O_4. The similar results were also observed in the spectrum of peptide **1**−Fe_3O_4 NP (Figure S8). These results suggest that the screened peptides (peptide **1** and peptide **2**) were successfully grafted onto Fe_3O_4 NPs.

Thermogravimetric analysis (TGA) was also carried out to validate the conjugation of peptides to Fe_3O_4 nanoparticles. TG curves of peptide **2** stacked with peptide **2**−Fe_3O_4 and pure Fe_3O_4 are shown in Figure 6a. The weight loss of samples before 100 °C was mainly because of the absorption of water on Fe_3O_4 nanoparticles. There are few weight losses in the TG curve of pure Fe_3O_4. The sharp weight loss in the case of pure peptide **2** around 270 °C is due to mainly the thermal decomposition of the compound. In the peptide **2**−Fe_3O_4 curve, a sheer dip in weight around 250 °C might be due to the thermal decomposition of peptide **2** grafted onto Fe_3O_4

https://doi.org/10.1021/acsomega.2c08092
ACS Omega 2023, 8, 8712−8721

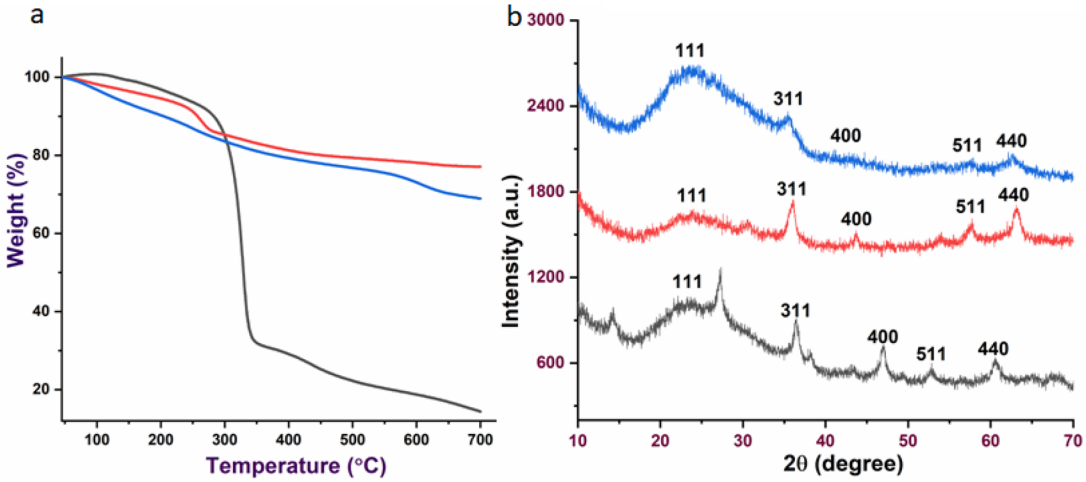

Figure 6. (a) TG curves of corresponding pure peptide **2** (black), peptide **2**−Fe_3O_4 nanoparticles (red), and pure Fe_3O_4 nanoparticles (blue). (b) PXRD patterns of pure Fe_3O_4 (black), peptide **1**−Fe_3O_4 nanoparticles (red), and peptide **2**−Fe_3O_4 nanoparticles (blue).

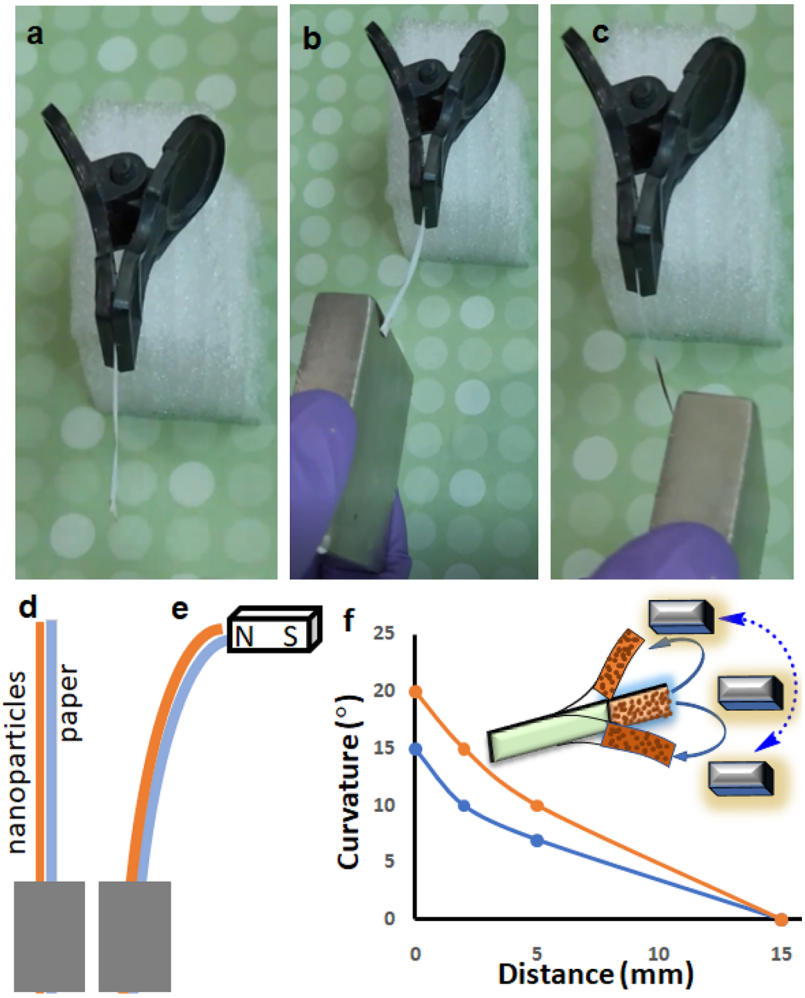

Figure 7. (a) Photograph of *α,ε*-hybrid peptide **1**-stabilized Fe_3O_4 nanoparticle-coated paper strip fixed by a clip. (b) Image showing the actuation under an external magnetic field. (c) Attraction of the Fe_3O_4 nanoparticles with an external magnet through paper. (d and e) Schematics of the magnetic-field-driven actuation property of the paper-based actuator. (f) Distance dependence of the curvature of the actuators. The blue line indicates raw paper and the orange line indicates nanoparticles.

nanoparticles, and after that no such change in weight probably resulted from the pure Fe_3O_4 nanoparticles. The same type of TG curve was observed for peptide **1** (Figure S9), suggesting the conjugation between the peptide and the Fe_3O_4 nanoparticles.

The formation of the magnetic nanoparticles was further confirmed by PXRD experiments. Figure 6b shows the stacked

https://doi.org/10.1021/acsomega.2c08092
ACS Omega 2023, 8, 8712−8721

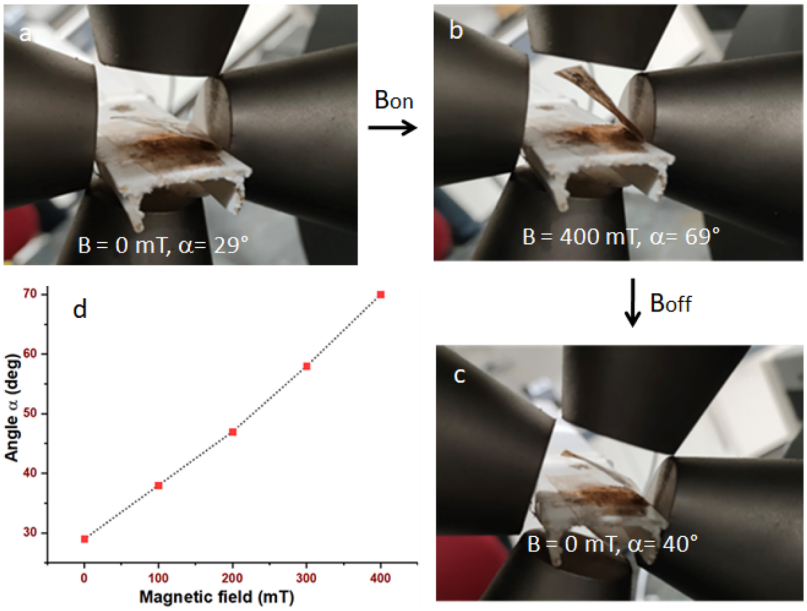

Figure 8. Images showing (a) the initial position (B = 0 T) of the paper, (b) the final state (B = 400 mT) of the actuation, and (c) the rest state after switching off the magnetic field. (d) Rotational angle (α) as a function of the applied magnetic field strength up to 400 mT.

PXRD patterns of α,ε-hybrid peptide-stabilized Fe_3O_4 nanoparticles and also pure Fe_3O_4 nanoparticles. The peak positions at 22.82 (111), 28.416 (220), 36.07 (311), 43.59 (400), 57.69 (511), and 63.21 (440) are close to that of magnetite (card no. 89-3854), i.e., standard Fe_3O_4 X-ray data. It is implied that the resultant Fe_3O_4 nanoparticles are pure Fe_3O_4 with a spinel structure and that grafting does not induce any phase change of Fe_3O_4.

Paper is a not magnetic material. It is mainly composed of cellulose fibers that have many oxygen-containing groups on the surface. Compared to other commonly used materials in the field of soft actuators, cellulose offers many advantages such as low cost, sustainability, versatile applications, and abundance.[35] Cellulose-based soft actuators are receiving a lot of attention and are undergoing exciting development due to the enormous and growing demand in the functional flexible electronics industry. We have coated both peptide-stabilized nanoparticles and pure Fe_3O_4 nanoparticles on the paper strip (Figure S10). The microstructures of peptide−-Fe_3O_4 nanoparticles are analyzed using scanning electron microscopy (SEM) (Figure S11) and energy-dispersive X-ray spectroscopy (EDS) (Figure S12). As a control, we compared the stability of a coating of pure Fe_3O_4 nanoparticles with the peptide-stabilized Fe_3O_4 nanoparticles on paper. Pure Fe_3O_4 nanoparticles can easily agglomerate and sedimentate due to their high specific surface area and surface activity.[32] As a result, the pure Fe_3O_4 nanoparticle-coated paper could not hold the nanoparticles to properly coat it. Peptide−Fe_3O_4 nanoparticles were more uniformly distributed on the raw paper due to the strong hydrophobic nature of the peptides, which can bind with the Fe_3O_4 nanoparticles to coat the paper in a more effective way (Supplementary Movie 1). The developed method for the one-pot synthesis of nitropeptides−Fe_3O_4 nanoparticles is very robust, and coated paper with the peptides−Fe_3O_4 nanoparticles is very stable for couple of months in open air under laboratory light and room temperature. We have shown the actuation property of peptide-stabilized Fe_3O_4 nanoparticles in two different magnetic environments. First, we applied a static magnetic field using a strong block magnet (B = 300 mT). (Supplementary Movie 2) To investigate the actuating property, 0.2 g of α,ε-hybrid peptide **1**−Fe_3O_4 nanoparticles suspended in methanol is coated uniformly on one side of a raw paper strip and placed in a static position with the help of a clam, and the whole system is placed in a nonmagnetic zone (Figure 7a). This coated paper can be used to construct magnet-sensitive actuators (Figure 7b and c). The magnetic-field-driven actuation mechanism of coated paper actuators is schematically illustrated in Figure 7d and e. In the initial state, the paper-based actuators are in a straight state. In the presence of magnet, the α,ε-hybrid peptide **1**-stabilized magnetic nanoparticle-coated paper tends to bend toward the magnet. The actuator performed a bending motion toward the magnet side. Even the actuators bend toward the magnet when the Fe_3O_4 nanoparticles are on the opposite side of the paper, though the bending curvature is less (Figure 7f). After the removal of the external magnet, the actuator can turn back to the initial state.

In the second case, we have shown actuation in the presence of a mobile magnetic field to elucidate the magnetically controllable shape-morphing mechanism. 0.3 g of peptide **2**−Fe_3O_4 nanoparticle suspended in methanol is coated uniformly on one side of a square butter paper (2 cm × 2 cm). The paper is folded and placed in a static position with the help of a clam, and the whole system is placed into a DXCG-5004 electromagnet. When the magnetic field was 0 T, the paper formed a rotational angle of 29° (Figure 8a). Upon actuation, the upper panel of magneto-origami paper rotates around the crease due to an increase in the magnetic field in the interval of 100 mT (Supplementary Movie 3), which finally leads the folded paper to make a final rotational angle of 69° (Figure 8b). After turning off the magnetic field totally from the system, the folded magneto origami paper does not fully revert back to its original position but finally make a rotational angle of 40° (Figure 8c). The change in rotational angle (α) is plotted against variant magnetic field in Figure 8d.

https://doi.org/10.1021/acsomega.2c08092
ACS Omega 2023, 8, 8712−8721

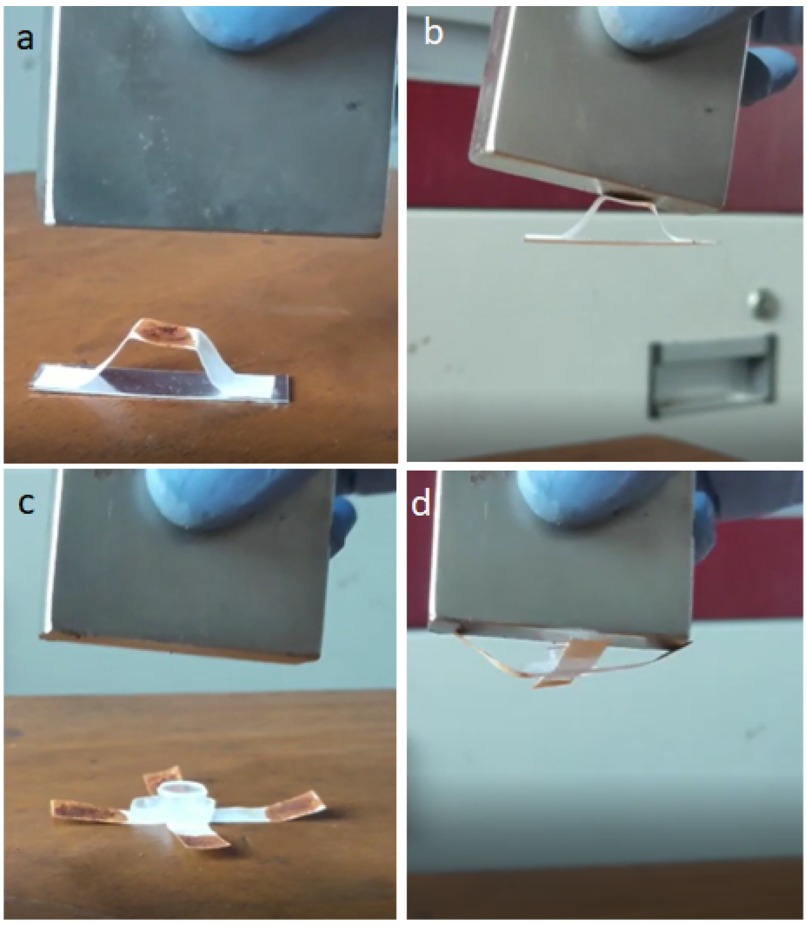

Figure 9. Images showing (a) the initial position (B = 0 T) and (b) the final state (B = 300 mT) of a paper-based origami showing hanger-like actuation, Images showing (c) the initial position (B = 0 T) and (d) the final state (B = 300 mT) of a paper-based origami showing the weight lifting property.

These peptide-stabilized Fe_3O_4 NP-based paper-based actuators can show the actuating property in different uses of day-to-day life. For this experiment, we have coated a raw paper in different ways to form two different paper-based actuators (Figure 9a and c). These two different patterns can show actuation after the application of an external magnetic field (B = 300 mT) using a block magnet. The arrangement in Figure 9a, in which a paper strip is glued on an aluminum plate at both ends and coated by peptide $-Fe_3O_4$ in the middle, can act as a hanger (Supplementary Movie 4) (Figure 9b) under an applied magnetic field. The arrangement in Figure 9c, in which a small weight was placed in the middle of specially patterned magneto origami, can uplift weight under an applied magnetic field (Supplementary Movie 5) (Figure 9d).

The excellent performance of paper-based actuators prototypes in various domains has been demonstrated.[35] However, there are some challenges for practical use and commercialization. There are issues with output capability, strength, stability, and durability under hoarse condition.[36] Several directions for further research and development are still attractive and flourishing.

CONCLUSIONS

In conclusion, we have discussed the development of α,ε-hybrid peptide-stabilized magnetic nanoparticles and their application to fabricate a paper-based actuators. From single-crystal X-ray diffraction analysis, the nitropeptide **2** has an extended structure with a *trans* geometry. The one-pot in situ multiple oxidation−reduction reaction of a synthetic nitro-peptide solution in ammonium hydroxide and $FeCl_2$ leads to the formation of Fe_3O_4 nanoparticles. The reduction reaction replaces the nitro group with an amine group, which finally acts as capping agent for the stabilization of the Fe_3O_4 nanoparticles. Paper-based soft magneto machines with multivariant actuation modes such as contraction−expansion, bending, and uplifting locomotion and real-life application has been studied. The device has potential as controllable paper-based soft robots.

ASSOCIATED CONTENT

Supporting Information

Supporting Information, , Figure S11 - S17, Scheme S1 and scheme S2, Supplementary movies 1−5. The Supporting Information (PDF) is available free of charge on the ACS Publications Web site. The Supporting Information is available free of charge at https://pubs.acs.org/doi/10.1021/acsomega.2c08092.

Synthesis and characterizations of peptides and ^1H NMR and ^{13}C NMR spectra (PDF)
Crystal structure of peptide **2** (CIF)
Comparison of Fe_3O_4 and peptide−Fe_3O_4 nanoparticle coatings (MP4)
Application of a static magnetic field using a strong block magnet (MP4)

https://doi.org/10.1021/acsomega.2c08092
ACS Omega 2023, 8, 8712−8721

Rotation of the upper panel of magneto-origami paper (MP4)

Hanger action of a paper strip coated with peptide **1**–Fe_3O_4 (MP4)

Use of magneto-origami paper to lift a weight under an applied magnetic field (MP4)

AUTHOR INFORMATION

Corresponding Author

Debasish Haldar − *Department of Chemical Sciences, Indian Institute of Science Education and Research Kolkata, Mohanpur, West Bengal 741246, India;* orcid.org/0000-0002-7983-4272; Email: deba_h76@yahoo.com

Authors

Ananda Shit − *Department of Chemical Sciences, Indian Institute of Science Education and Research Kolkata, Mohanpur, West Bengal 741246, India*

Surajit Singh − *Department of Chemical Sciences, Indian Institute of Science Education and Research Kolkata, Mohanpur, West Bengal 741246, India*

Olamilekan Joseph Ibukun − *Department of Chemical Sciences, Indian Institute of Science Education and Research Kolkata, Mohanpur, West Bengal 741246, India*

Milan Gumtya − *Department of Chemical Sciences, Indian Institute of Science Education and Research Kolkata, Mohanpur, West Bengal 741246, India*

Complete contact information is available at: https://pubs.acs.org/10.1021/acsomega.2c08092

Author Contributions

A.S. synthesized the compounds and performed the experiments. S.S., O.J.I., and M.G. performed the experimental work. D.H. performed done the analysis and wrote the manuscript.

Notes

The authors declare no competing financial interest.

ACKNOWLEDGMENTS

A.S. is thankful to UGC, India, for the senior research fellowship. S.S. and M.G. thank CSIR, India, for fellowships. O.J.I. thanks IISER Kolkata for a fellowship. We thank IISER Kolkata for analytical facilities. This research was funded by CSIR, India (project no. 02/(0404)/21/EMR-II).

REFERENCES

(1) Apsite, I.; Salehi, S.; Ionov, L. Materials for Smart Soft Actuator Systems. *Chem. Rev.* **2022**, *122*, 1349−1415.

(2) Yi, S.; Wang, L.; Chen, Z.; Wang, J.; Song, X.; Liu, P.; Zhang, Y.; Luo, Q.; Peng, L.; Wu, Z.; Guo, C. F.; Jiang, L. High-Throughput Fabrication of Soft Magneto-Origami Machines. *Nat. Commun.* **2022**, *13*, 4177.

(3) Chen, D.; Pei, Q. Electronic Muscles and Skins: A Review of Soft Sensors and Actuators. *Chem. Rev.* **2017**, *117*, 11239−11268.

(4) Dattler, D.; Fuks, G.; Heiser, J.; Moulin, E.; Perrot, A.; Yao, X.; Giuseppone, N. Design of Collective Motions from Synthetic Molecular Switches, Rotors, and Motors. *Chem. Rev.* **2020**, *120*, 310−433.

(5) Zheng, Z.; Wang, H.; Dong, L.; Shi, Q.; Li, J.; Sun, T.; Huang, Q.; Fukuda, T. Ionic Shape-Morphing Microrobotic End-Effectors for Environmentally Adaptive Targeting, Releasing, and Sampling. *Nat. Commun.* **2021**, *12*, 411.

(6) Liu, X.; Li, J.; Gui, B.; Lin, G.; Fu, Q.; Yin, S.; Liu, X.; Sun, J.; Wang, C. A Crystalline Three-Dimensional Covalent Organic Framework with Flexible Building Blocks. *J. Am. Chem. Soc.* **2021**, *143*, 2123−2129.

(7) Wang, H.; Yang, Y.; Zhang, M.; Wang, Q.; Xia, K.; Yin, Z.; Wei, Y.; Ji, Y.; Zhang, Y. Electricity-Triggered Self-Healing of Conductive and Thermostable Vitrimer Enabled by Paving Aligned Carbon Nanotubes. *ACS Appl. Mater. Interfaces* **2020**, *12*, 14315−14322.

(8) Huang, Y.; Bisoyi, H. K.; Huang, S.; Wang, M.; Chen, X. M.; Liu, Z.; Yang, H.; Li, Q. Bioinspired Synergistic Photochromic Luminescence and Programmable Liquid Crystal Actuators. *Angew. Chemie - Int. Ed.* **2021**, *60*, 11247−11251.

(9) Su, Y.; Qiu, T.; Song, W.; Han, X.; Sun, M.; Wang, Z.; Xie, H.; Dong, M.; Chen, M. Melt Electrospinning Writing of Magnetic Microrobots. *Adv. Sci.* **2021**, *8*, 2003177.

(10) Zhou, S.; Cun, F.; Zhang, Y.; Zhang, L.; Yan, Q.; Sun, Y.; Huang, W. Thermo-Responsive Aluminum-Based Polymer Composite Films with Controllable Deformation. *J. Mater. Chem. C* **2019**, *7*, 7609−7617.

(11) Dingler, C.; Müller, H.; Wieland, M.; Fauser, D.; Steeb, H.; Ludwigs, S. From Understanding Mechanical Behavior to Curvature Prediction of Humidity-Triggered Bilayer Actuators. *Adv. Mater.* **2021**, *33*, 2007982−2007991.

(12) Song, S.; Zhang, C.; Wang, J.; Li, W.; Jiang, Z.; Zhang, Y. High-Performance Nacre-like Graphene@polymer Supported Montmorillonite Composite Actuator and Sensor. *Sensors Actuators, B Chem.* **2021**, *332*, 129446.

(13) Li, C.; Lau, G. C.; Yuan, H.; Aggarwal, A.; Dominguez, V. L.; Liu, S.; Sai, H.; Palmer, L. C.; Sather, N. A.; Pearson, T. J.; Freedman, D. E.; Amiri, P. K.; de la Cruz, M. O.; Stupp, S. I. Fast and Programmable Locomotion of Hydrogel-Metal Hybrids under Light and Magnetic Fields. *Sci. Robot.* **2020**, *5*, No. eabb9822, DOI: 10.1126/scirobotics.abb9822.

(14) Gao, T.; Xu, G.; Wen, Y.; Cheng, H.; Li, C.; Qu, L. An Intelligent Film Actuator with Multi-Level Deformation Behaviour. *Nanoscale Horizons* **2020**, *5*, 1226−1232.

(15) Khodambashi, R.; Alsaid, Y.; Rico, R.; Marvi, H.; Peet, M. M.; Fisher, R. E.; Berman, S.; He, X.; Aukes, D. M. Heterogeneous Hydrogel Structures with Spatiotemporal Reconfigurability Using Addressable and Tunable Voxels. *Adv. Mater.* **2021**, *33*, 2005906.

(16) Kotal, M.; Tabassian, R.; Roy, S.; Oh, S.; Oh, I. K. Metal-Organic Framework-Derived Graphitic Nanoribbons Anchored on Graphene for Electroionic Artificial Muscles. *Adv. Funct. Mater.* **2020**, *30*, 1910326.

(17) Xia, Y.; He, Y.; Zhang, F.; Liu, Y.; Leng, J. A Review of Shape Memory Polymers and Composites: Mechanisms, Materials, and Applications. *Adv. Mater.* **2021**, *33*, 2000713.

(18) Li, G.; Chen, X.; Zhou, F.; Liang, Y.; Xiao, Y.; Cao, X.; Zhang, Z.; Zhang, M.; Wu, B.; Yin, S.; Xu, Y.; Fan, H.; Chen, Z.; Song, W.; Yang, W.; Pan, B.; Hou, J.; Zou, W.; He, S.; Yang, X.; Mao, G.; Jia, Z.; Zhou, H.; Li, T.; Qu, S.; Xu, Z.; Huang, Z.; Luo, Y.; Xie, T.; Gu, J.; Zhu, S.; Yang, W. Self-Powered Soft Robot in the Mariana Trench. *Nature* **2021**, *591*, 66−71.

(19) Bhunia, S.; Chandel, S.; Karan, S. K.; Dey, S.; Tiwari, A.; Das, S.; Kumar, N.; Chowdhury, R.; Mondal, S.; Ghosh, I.; Mondal, A.; Khatua, B. B.; Ghosh, N.; Reddy, C. M. Autonomous Self-Repair in Piezoelectric Molecular Crystals. *Science* **2021**, *373*, 321−327.

(20) Shen, Z.; Chen, F.; Zhu, X.; Yong, K. T.; Gu, G. Stimuli-Responsive Functional Materials for Soft Robotics. *J. Mater. Chem. B* **2020**, *8*, 8972−8991.

(21) Karnaushenko, D.; Kang, T.; Bandari, V. K.; Zhu, F.; Schmidt, O. G. 3D Self-Assembled Microelectronic Devices: Concepts, Materials, Applications. *Adv. Mater.* **2020**, *32*, 1902994.

(22) Stoddart, J. F. Mechanically Interlocked Molecules (MIMs)—Molecular Shuttles, Switches, and Machines (Nobel Lecture). *Angew. Chemie - Int. Ed.* **2017**, *56*, 11094−11125.

(23) Feringa, B. L. The Art of Building Small: From Molecular Switches to Motors (Nobel Lecture). *Angew. Chemie - Int. Ed.* **2017**, *56*, 11060−11078.

(24) *Foldamers: Structure, Properties and Applications*; Hecht, S., Huc, I., Eds.; John Wiley & Sons, 2007.

(25) Gellman, S. H. Foldamers: A Manifesto. *Acc. Chem. Res.* **1998**, *31*, 173−180.
(26) Hill, D. J.; Mio, M. J.; Prince, R. B.; Hughes, T. S.; Moore, J. S. A Field Guide to Foldamers. *Chem. Rev.* **2001**, *101*, 3893−4011.
(27) Karle, I. L.; Pramanik, A.; Banerjee, A.; Bhattacharjya, S.; Balaram, P. ω-Amino Acids in Peptide Design. Crystal Structures and Solution Conformations of Peptide Helices Containing a β-Alanyl-γ-Aminobutyryl Segment. *J. Am. Chem. Soc.* **1997**, *119*, 9087−9095.
(28) Roy, R. S.; Gopi, H. N.; Raghothama, S.; Karle, I. L.; Balaram, P. Hybrid Peptide Hairpins Containing A-and Ω-Amino Acids: Conformational Analysis of Decapeptides with Unsubstituted β-, γ-, and δ-Residues at Positions 3 and 8. *Chem. Eur. J.* **2006**, *12*, 3295−3302.
(29) Rai, R.; Vasudev, P. G.; Ananda, K.; Raghothama, S.; Shamala, N.; Karle, I. L.; Balaram, P. Hybrid Peptides: Expanding the β Turn in Peptide Hairpins by the Insertion of β-, γ-, and δ-Residues. *Chem. - A Eur. J.* **2007**, *13*, 5917−5926.
(30) Ganesh Kumar, M.; Thombare, V. J.; Katariya, M. M.; Veeresh, K.; Raja, K. M. P.; Gopi, H. N. Non-Classical Helices with Cis Carbon-Carbon Double Bonds in the Backbone: Structural Features of α,γ-Hybrid Peptide Foldamers. *Angew. Chemie - Int. Ed.* **2016**, *55*, 7847−7851.
(31) Debnath, M.; Abbasi, M.; Sasmal, S.; Datta, R.; Haldar, D. M-Nitrocinnamic Acid Containing Lipophilic Peptide Exhibits Selective Growth Inhibition Activity against Leishmania Major. *ChemistrySelect* **2019**, *4* (1), 116−122.
(32) Wang, X.; Han, B.; Yu, R. P.; Li, C. H.; Zhao, Z. Y.; Zhang, Q. C.; Lu, T. J. Magnetic-responsive Fe3O4 Nanoparticle-impregnated cellulose paper actuators. *Extrem. Mech. Lett.* **2018**, *25*, 53−59.
(33) Sarkar, R.; Sasmal, S.; Podder, D.; Haldar, D. Solvent Assisted Room Temperature Synthesis of Magnetically Retrievable and Reusable Dipeptide Stabilized Nanocrystals for Suzuki-Miyaura Cross-Coupling. *Macromol. Symp.* **2016**, *369*, 67−73.
(34) You, F.; Yin, G.; Pu, X.; Li, Y.; Hu, Y.; Huang, Z.; Liao, X.; Yao, Y.; Chen, X. Biopanning and Characterization of Peptides with Fe_3O_4 Nanoparticles-Binding Capability via Phage Display Random Peptide Library Technique. *Colloids Surfaces B Biointerfaces* **2016**, *141*, 537−545.
(35) Liu, Y.; Shang, S.; Mo, S.; Wang, P.; Yin, B.; Wei, J. Soft Actuators Built from Cellulose Paper: A Review on Actuation, Material, Fabrication, and Applications. *J. Sci. Adv. Mater. Devices* **2021**, *6*, 321−337.
(36) Zhu, J.; He, J.; Du, X.; Lu, R.; Huang, L.; Ge, X. A Facile and Flexible Process of β-Cyclodextrin Grafted on Fe_3O_4 Magnetic Nanoparticles and Host-Guest Inclusion Studies. *Appl. Surf. Sci.* **2011**, *257* (21), 9056−9062.

https://doi.org/10.1021/acsomega.2c08092
ACS Omega 2023, 8, 8712−8721